


Article

Low-Power pH Sensor Based on Narrow Channel Open-Gated $\text{Al}_{0.25}\text{Ga}_{0.75}\text{N}/\text{GaN}$ HEMT and Package Integrated Polydimethylsiloxane Microchannels

Xianghong Yang, Jiawei Ao, Sichen Wu, Shenhui Ma, Xin Li *, Long Hu, Weihua Liu  and Chuanyu Han

School of Microelectronics, Xi'an Jiaotong University, Xi'an 710049, China; yxh8000@stu.xjtu.edu.cn (X.Y.); ajp2269228624@stu.xjtu.edu.cn (J.A.); wusichen54@stu.xjtu.edu.cn (S.W.); hasfryma.879@stu.xjtu.edu.cn (S.M.); hulong@xjtu.edu.cn (L.H.); lwhua@mail.xjtu.edu.cn (W.L.); hanchuanyu@mail.xjtu.edu.cn (C.H.)

* Correspondence: lx@mail.xjtu.edu.cn; Tel.: +86-29-8266-3343

Received: 15 October 2020; Accepted: 19 November 2020; Published: 22 November 2020



Abstract: pH sensors with low-power and strong anti-interference are extremely important for industrial online real-time detection. Herein, a narrow channel pH sensor based on $\text{Al}_{0.25}\text{Ga}_{0.75}\text{N}/\text{GaN}$ high electron mobility transistor (HEMT) with package integrated Polydimethylsiloxane (PDMS) microchannels is proposed. The fabricated device has shown potential advantages in improving stability and reducing power consumption in response to pH changes of the solution. The performance of the pH sensor was demonstrated where the preliminary results showed an ultra-low power ($<5.0 \mu\text{W}$) at $V_{\text{DS}} = 1.0 \text{ V}$. Meanwhile, the sensitivity was $0.06 \mu\text{A}/\text{V}\cdot\text{pH}$ in the range of $\text{pH} = 2$ to $\text{pH} = 10$, and the resolution of the sensor was 0.1 pH . The improvement in performance of the proposed sensor can be related to the narrow channel and microchannel, which can be attributed to better surface Ga_xO_y in a microchannel with larger H^+ and HO^- concentration on the sensing surface during the detection process. The low-power sensor with excellent stability can be widely used in various unattended or harsh environments, and it is more conducive to integration and intelligence, which lays the foundation for online monitoring in vivo.

Keywords: $\text{Al}_{0.25}\text{Ga}_{0.75}\text{N}/\text{GaN}$ HEMT; narrow channel; microchannel; pH detection

1. Introduction

Biosensor is an interdisciplinary organic combination of bioactive materials (enzymes, proteins, desoxyribonucleic acid (DNA), antibodies, antigens, biofilms, etc.) and electrochemical transducers [1–3]. It is an advanced detection method essential for the development of biotechnology and the monitoring method is also fast since the micro-analysis method is at the molecular level of the substance [4]. Biosensor technology will surely be a new growth point between information and biotechnology [5]. It has broad application prospects, namely, clinical diagnosis, industrial control, food and drug analysis (including biopharmaceutical research and development) in the national economy, environmental protection, biotechnology, biochips, and other research areas. With the development of science and technology, biotechnology and electronics infiltrate and merge ulteriorly, therefore more and more electrochemical biosensors have been designed to solve the detection problem of ultra-low concentration [6–8].

Among the different kinds of biosensors, aluminum gallium nitride/gallium nitride high electron mobility transistor ($\text{AlGaIn}/\text{GaIn}$ HEMT) based devices stand out for their ultra-high sensitivity, fast response speed, and harsh environment adaptability. In addition, it has superior biocompatibility and non-toxicity because of the properties of the III–V nitride materials [9–12], a controllable surface

stoichiometry such as high two-dimensional electronic gas (2DEG) density at the AlGaIn/GaN hetero-interface, larger band gap, high breakdown voltage, high electron mobility, and stable chemical properties [13–17]. The AlGaIn/GaN HEMT-based biosensor can detect different targets such as ions [18–20], DNA [21–23], protein [24–26], glucose [27,28], prostate specific antigen (PSA) [29–31], and cellular response [32], etc. Even without any functionalization, the bare AlGaIn surface (open-gated) is especially sensitive to the pH change in the solution. The measurement of pH is needed in many different applications including medicine, biology, chemistry, food science, environmental science, and oceanography. The HEMT-based pH sensor performance depends not only on high-quality AlGaIn/GaN heterojunction epitaxial wafers, but also on the structure parameters of the sensitive area and the type and quality of surface sensitive materials. In 2003, G. Steinhof et al. [33] researched the ion sensitivity of native metal oxide on the III-nitride surface, and found a linear response when the pH changed from pH = 2 to pH = 12 for both as-deposited and thermally oxidized GaN surfaces. In 2007, Kang et al. [34] found the use of a Sc_2O_3 gate dielectric produced superior results to either a native oxide or UV ozone-induced oxide in the gate region. In 2015, Chen et al. [35] fabricated and studied a GaN-based pH sensor prepared by a hydrogen peroxide (H_2O_2) treatment to increase the thickness of the Ga_xO_y . In 2015, Lee et al. [27] used a photoelectrochemical (PEC) etching method to grow a ZnO-based nanorod array on the recessed gate of the AlGaIn/GaN HEMT sensor to improve device performance. Dong et al. [36] developed an idea to improve the sensitivity of pH sensors based on AlGaIn/GaN HEMT by introducing multi-sensing segments in 2018. Li et al. [37] fabricated a normally off AlGaIn/GaN HEMT through the photoelectrochemical (PEC) method for a pH sensor application in 2019.

However, the HEMT-based pH sensors reported in the literature have a large channel width-to-length ratio (W/L), and does not consider power consumption and environmental interference. Additionally, the larger sensitive area is also not conducive to the miniaturization and integration of sensors. Thus, HEMT-based pH sensor with a particularly small W/L is highly interesting. The W/L of the sensitive channel is critical to the performance of the HEMT-based pH sensor. Theoretically, the output current of the HEMT is inversely proportional to the W of the device, so a larger sensitive area and larger W/L can increase the output current and sensitivity. However, long-term exposure of the large sensitive area to the air will reduce the stability and increase interference from environmental uncertainties and power consumption, which are exactly what small channels can avoid, especially the sensitive area of the biosensor that is directly exposed to the liquid under detection. Therefore, it is of great significance if we can not only overcome the difficulty of small channels, but also integrate wide channel devices on the same chip and reduce power consumption and improve anti-interference ability.

Herein, in order to improve the stability and reduce the power consumption of the sensor, we tried to study a narrow channel width open-gated $\text{Al}_{0.25}\text{Ga}_{0.75}\text{N}/\text{GaN}$ HEMT-based pH sensor with package integrated Polydimethylsiloxane (PDMS) microchannels in this paper, which can minimize the external environment interference and ensure the device is not polluted by dust. The unique physical properties and high sensitivity of GaN hetero-junctions to surface charges are used as a tool to distinguish the pH level of the solution. The narrow channel width with microchannels can inherently reduce power consumption and enhance anti-interference. The cost of open-gated is low and changes in sensitive area charge and surface potential are easily controlled by 2DEG and avoid gate leakage power consumption in response to the pH of the solution change. On the other hand, we tried to integrate 30 biosensors on a $2\text{ cm} \times 2\text{ cm}$ epitaxial substrate. The devices with different channels can be used for pH measurement with different accuracy. The miniaturization of devices is one of the necessary conditions for biochips, and the maturation of the crafts we proposed is an important part of integration, which means to reduce the aspect ratio of the device while ensuring the sensitivity is of great significance. Thus, this research can improve the development of sensors in the direction of miniaturization, integration, and intelligence.

2. Basic Structure and Operation Principle

2.1. Basic Structure

The schematic configuration of the fabricated open-gated $\text{Al}_{0.25}\text{Ga}_{0.75}\text{N}/\text{GaN}$ HEMT pH sensor is shown in Figure 1. The sensitive area is located between the source and drain, and no metal deposition is required (that is, no Schottky contact is made), so it is called a “open-gated” HEMT pH sensor. The epitaxial structure (NTT Advanced Technology Cor., Tokyo, Japan) is composed of multiple layers of materials by the metal organic chemical vapor deposition (MOCVD) such as silicon substrate, 3.9- μm carbon doped (C-doped) GaN buffer layer, 300-nm GaN layer, 1-nm aluminum nitride (AlN) insert layer, 20-nm $\text{Al}_{0.25}\text{Ga}_{0.75}\text{N}$ barrier layer, and 2 nm-GaN cap layer. Unlike the traditional HEMT with only AlGaN barrier layer, the GaN channel layer on the substrate, the sensor in this work was fabricated with an AlN insert layer and GaN cap layer. The insert layer can increase the effective conduction band offset of the AlGaN barrier layer and the GaN channel layer. On one hand, it can form a deeper and narrower quantum well because the AlN has a large band gap E_g , which is beneficial to increase the 2DEG concentration in the channel. On the other hand, it can also suppress the disordered scattering of the alloy on the part where 2DEG penetrates into the AlGaN barrier layer, improving the channel electron mobility. The GaN cap layer can increase the Schottky barrier on the AlGaN/GaN heterojunction structure, thus reducing gate leakage and power consumption of the sensor. Ti/Al/Ni/Au (30/180/40/50 nm) was deposited as the source and drain electrode to form an Ohmic contact on the GaN cap layer by electron-beam evaporation. The width and length of the channel sensitive region were W (50 μm , 5 μm , and 3 μm) and L (900 μm), respectively. This sensitive area was exposed to the tested solution by photolithography and the rest was passivated with SU-8.

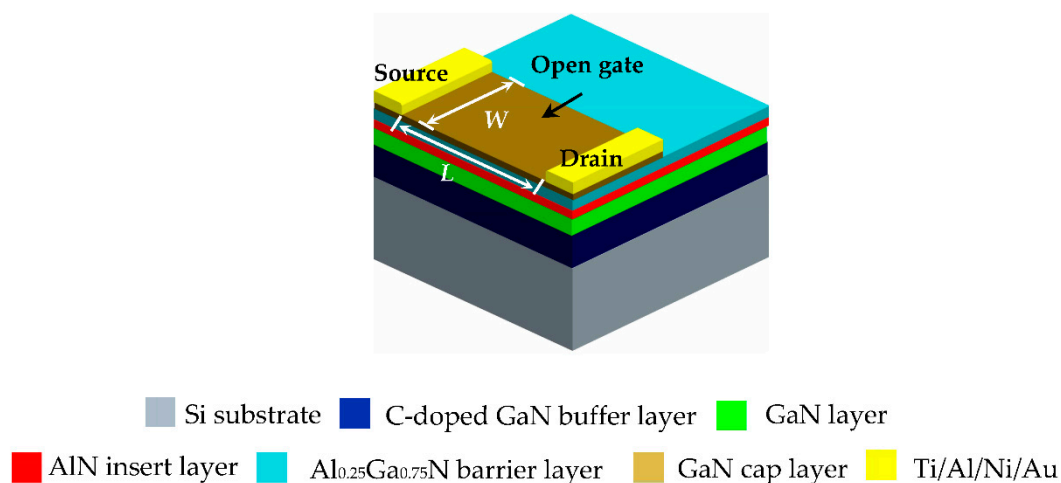
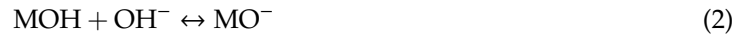


Figure 1. The schematic configuration of the open-gated $\text{Al}_{0.25}\text{Ga}_{0.75}\text{N}/\text{GaN}$ HEMT-based pH sensor.

2.2. Operation Principle

A site-binding model that was initially proposed for the oxide/aqueous sensing mechanism is currently in use to explain the sensing principle for AlGaN/GaN HEMT-based pH sensors [38,39] because a natural oxide layer (such as Al_xO_y and Ga_xO_y) is formed on the surface of the AlGaN and GaN layer when the device is exposed in air [33]. Figure 2 presents the operating principle of the proposed HEMT-based pH sensor. According to the site-binding model, the adsorption of protons or hydroxyl ions by surface hydroxyl groups results in positive or negative sites on the Ga_xO_y surface. 2DEG density in the channel is balanced to the surface states of the GaN surface (the cap layer in our case). Therefore, the adsorption of positive or negative charges on the $\text{Ga}_x\text{O}_y/\text{GaN}$ surface can

change the surface charge state as well as the surface potential, thus altering the 2DEG density [36]. The relevant reactions mechanisms are as follows.



where MOH is the hydroxyl groups and M represents Al and Ga due to the Ga-face growth. When testing in the solution of low pH (acid solutions) (i.e., the concentration of H^+ is larger than that of OH^- ($N_{\text{H}^+} > N_{\text{OH}^-}$)), the GaOH groups tend to accept a proton and become protonated hydroxyls GaOH_2^+ that act as acceptors, represented by Equation (1). Therefore, the GaN surface becomes positively charged [40], leading to the increased sheet carrier density in the 2DEG channel, which finally results in the increase of drain-source current (I_{DS}). Similarly, when testing in the solution of high pH (alkaline solutions), the concentration of OH^- was higher than that of H^+ ($N_{\text{H}^+} < N_{\text{OH}^-}$), therefore GaOH groups release proton and become GaO^- that acts as donors, represented by Equation (2). Hence, the GaN surface was negatively charged, resulting in the reduced sheet carrier density in the 2DEG channel, which leads to the decreased I_{DS} . In Figure 2, I_{DS} is the initial current of $\text{Al}_{0.25}\text{Ga}_{0.75}\text{N}/\text{GaN}$ HEMT, and ΔI_{DS} is the output current of the sensor under a certain pH solution when source-drain voltage (V_{DS}) is constant. The H^+ and OH^- presented in Figure 2, respectively represent the concentration of hydrogen ions and hydroxide ions in the solution.

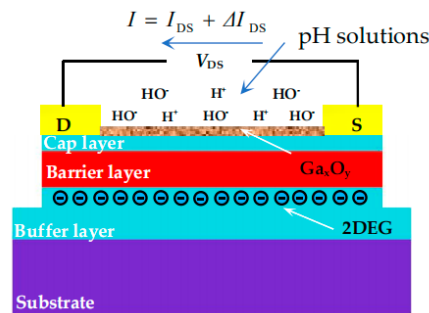


Figure 2. The operation principle of the open-gated $\text{Al}_{0.25}\text{Ga}_{0.75}\text{N}/\text{GaN}$ HEMT-based pH sensor.

3. Fabrication Technology

Since the surface of the open-gated HEMT is very close to the $\text{Al}_{0.25}\text{Ga}_{0.75}\text{N}/\text{GaN}$ inter-junction 2DEG channel, the surface charge or potential change in the sensitive area can better control the 2DEG concentration in $\text{Al}_{0.25}\text{Ga}_{0.75}\text{N}/\text{GaN}$ hetero-junction. The output current of the HEMT is inversely proportional to the channel width of the GaN HEMT, and a larger sensitive area and larger W/L can increase the output current and sensitivity theoretically. However, long-term exposure of the large sensitive area in the air will reduce the stability and increase the interference of water molecules. At the same time, the larger output current will increase the power consumption of the device. Therefore, we designed and manufactured a narrow channel open-gated HEMT-based pH sensor, and the 3D schematic of individual $\text{Al}_{0.25}\text{Ga}_{0.75}\text{N}/\text{GaN}$ HEMT device is shown in Figure 1. Since we used the same sensor layout with previously fabricated nanoribbon-based ion-sensitive field-effect transistors (NR-ISFETs) [41,42], there were also three types of HEMT devices in one chip whose channel lengths were all $L = 900 \mu\text{m}$, and channel widths were $W = 3 \mu\text{m}$, $5 \mu\text{m}$, and $50 \mu\text{m}$, respectively. Based on an epitaxial wafer on the Si substrate, Ohmic contacts of metals on the GaN cap layer were formed, which are regarded as the source and drain terminals. The main fabrication processes are described in Figure 3, where the detailed manufacturing steps are as follows:

- (1) Cleaning the epitaxial wafer: The original $\text{Al}_{0.25}\text{Ga}_{0.75}\text{N}/\text{GaN}$ epitaxial wafer on the Si substrate (NTT Advanced Technology Cor., Figure 3a) is composed of a p-type low resistivity Si substrate, GaN buffer layer ($3.9 \mu\text{m}$ -C-doped), GaN layer (300 nm), AlN layer (1 nm), $\text{Al}_{0.25}\text{Ga}_{0.75}\text{N}$

- barrier layer (20 nm), and GaN cap layer (2 nm). Ultrasonically clean with acetone, isopropanol, and ethanol for 3 min, rinse with a large amount of deionized water, and blow dry with nitrogen.
- (2) Ion implantation to achieve isolation: First use AZ-5214E photoresist lithography to prepare ion implantation patterns, where the detailed steps are: (1) photoresist spin coating: keep the homogenizer at 1000 rpm for 10 s and 2000 rpm for 30 s, respectively; (2) pre-baking: keep the device at 110 °C for 70 s; (3) align exposure: exposure time of 7 s; (4) Developing: Immerse the device in a solution of AZ-400K: deionized water = 1:3 for 60 s; (5) ion implantation: The ion implantation process was completed at the Institute of Semiconductors, Chinese Academy of Sciences. The ion type was Ar^+ , the energy was 30/40/60/80 keV in turn, and the dose was $5.0 \times 10^{13}/\text{cm}^2$ (Figure 3b).
 - (3) Ohmic contact and pads: After cleaning the wafer, another photolithography was conducted (which lithography process is the same as that of ion implantation lithography), followed by the deposition of Ti/Al/Ni/Au (30/180/40/50 nm) in sequence by electron-beam evaporation (Ohmiker-50BR, Cello Technology Co. Ltd., Taiwan, China). The pads were prepared by magnetron sputtering (MSP-300B, Weinaworld Co. Ltd., Beijing, China), Ti/Au: 20/100 nm. Then, the lift-off process was carried out to form the Ohmic metal contacts of the source/drain regions, interconnect, and pads (Figure 3c).
 - (4) Finally, a 2 μm thick SU-8 photoresist layer (GM 1040, Gersteltec Sarl. Inc., Pully, Switzerland) was coated and patterned as the top passivation layer to prevent the metals from erosion by the liquid during testing (Figure 3d), and the sensing regions over the channel and only the pads were exposed. The process is listed as follows: (1) photoresist spin coating: keep the homogenizer at 1600 rpm for 40 s; (2) relax the device for 5 min at room temperature; (3) pre-baking: keep the device at 65 °C for 5 min, then 95 °C for 5 min, then slowly cool down to 23 °C, cooling time should be longer than 2 h; (4) exposure: exposure time is 32 s; (5) post-baking: keep the device at 65 °C for 5 min, then 95 °C for 5 min, then slowly cool down to 23 °C, cooling time should be longer than 4 h; (6) developing: immerse the device in propylene glycol monomethyl ether acetate (PGMEA) developer for 1 min; (7) hard-baking: keep the device at 135 °C for 2 h.

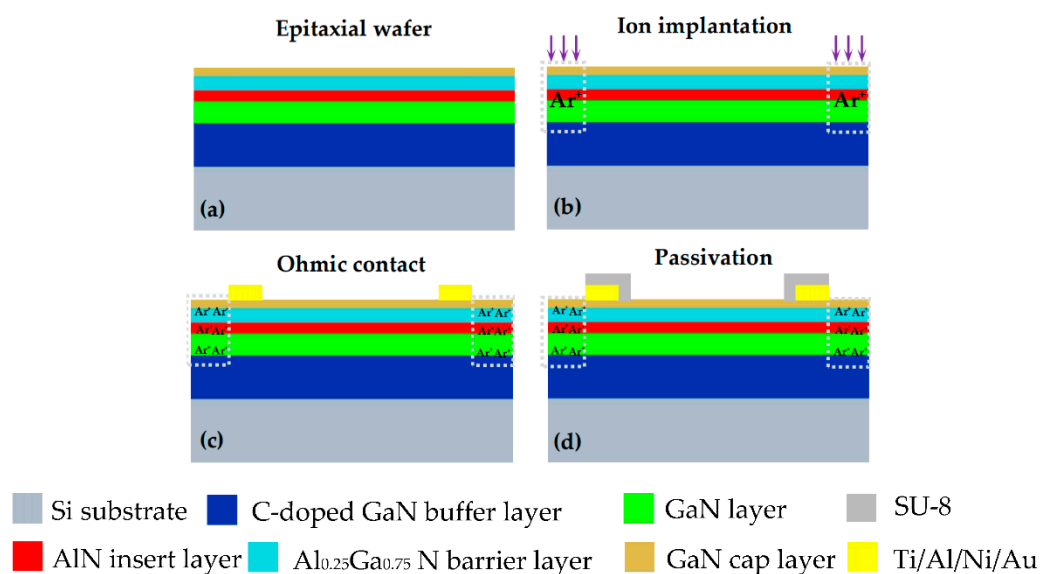


Figure 3. The fabrication process of the open-gated $\text{Al}_{0.25}\text{Ga}_{0.75}\text{N}/\text{GaN}$ HEMT-based pH sensor: (a) GaN epitaxial wafer on the Si substrate; (b) Ion implantation; (c) Ohmic contact metal: Ti/Al/Ni/Au; (d) SU-8 passivation layer.

The photograph of the open-gated $\text{Al}_{0.25}\text{Ga}_{0.75}\text{N}/\text{GaN}$ HEMT-based pH sensor after fabrication is shown in Figure 4a. Figure 4b presents the microscope image of the sensor chip, from the top to the bottom of the figure, where the channel widths were $W = 50\text{ }\mu\text{m}$, $5\text{ }\mu\text{m}$, and $3\text{ }\mu\text{m}$.

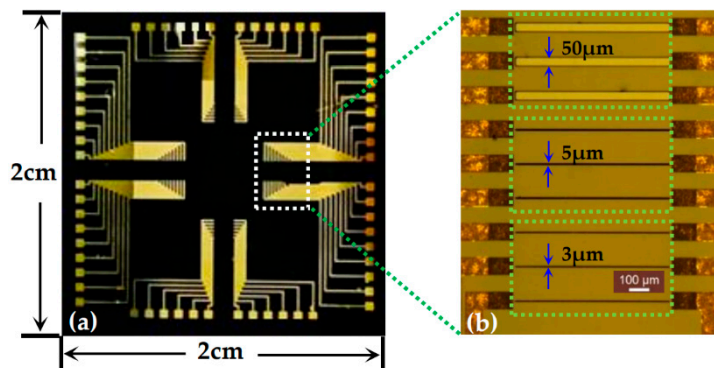


Figure 4. The photograph of the open-gated $\text{Al}_{0.25}\text{Ga}_{0.75}\text{N}/\text{GaN}$ HEMT-based pH sensor: (a) photograph of the sensor chip; (b) microscope image of the sensor chip.

4. Results and Discussion

The pH sensitive characteristics of the proposed sensor were studied by the revolving microprobe stage and semiconductor parameter analyzer (Keithley 4200A-SCS), as shown in Figure 5a. Figure 5b shows the fabricated open-gated $\text{Al}_{0.25}\text{Ga}_{0.75}\text{N}/\text{GaN}$ HEMT chip integrated with PDMS-based microchannels for pH sensing, this includes outlet and inlet parts for acidic, alkaline, and neutral solutions and a polymethyl methacrylate (PMMA) removable plate for fixing and replacing the chip. The PDMS microchannels are shown in Figure 5c, which were fabricated by coating and patterning of SU-8 on a Si substrate with a thickness of $10\text{ }\mu\text{m}$.

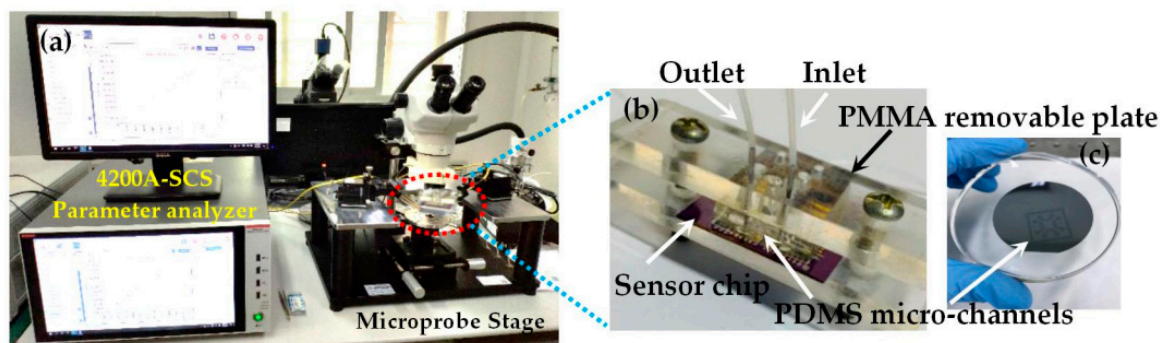


Figure 5. The testing platform of the open-gated $\text{Al}_{0.25}\text{Ga}_{0.75}\text{N}/\text{GaN}$ HEMT-based pH sensor: (a) testing platform; (b) photograph of the packaged pH sensor; (c) polydimethylsiloxane (PDMS)-based microchannels.

The injection and withdrawal of the pH solution uses a medical syringe with controllable flow. After the open-gated $\text{Al}_{0.25}\text{Ga}_{0.75}\text{N}/\text{GaN}$ HEMT-based pH sensor system was built, we performed the input and output characteristics ($I_{\text{DS}}-V_{\text{DS}}$ without pH solutions) of $\text{Al}_{0.25}\text{Ga}_{0.75}\text{N}/\text{GaN}$ HEMT with different channel widths ($W = 3\text{ }\mu\text{m}$, $5\text{ }\mu\text{m}$, $50\text{ }\mu\text{m}$) under channel length $L = 900\text{ }\mu\text{m}$ first, which is shown in Figure 6. In the range of $V_{\text{DS}} = 0$ to 2.0 V , the I_{DS} increased as W/L increased, and the sensor had a larger output current when $W = 50\text{ }\mu\text{m}$ compared with the other two sensors, which is consistent with the theory.

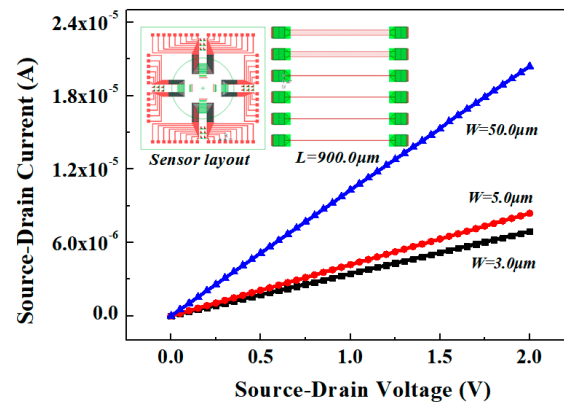


Figure 6. The output characteristics (I_{DS} - V_{DS}) of $\text{Al}_{0.25}\text{Ga}_{0.75}\text{N}/\text{GaN}$ HEMT with different channel widths ($W = 50 \mu\text{m}$, $5 \mu\text{m}$, $3 \mu\text{m}$) without pH solutions.

Although a larger W means that the sensitive channel area of the sensor is increased, it will also increase the instability of the sensor due to the exposed air, so that it cannot meet the detection of polar solutions in various unattended or harsh environments. The output signal of the sensor is small and can be amplified by the subsequent signal processing circuit, but its stability and anti-interference ability are derived from its own performance.

Subsequently, we studied the pH sensitivity of the HEMT-based sensor. The different pH solutions were obtained by diluting deionized water with hydrochloric acid (HCl) and sodium hydroxide (NaOH), which were used in the liquid testing and delivered to open-gated HEMT sensitive surface through the microchannels. According to theory and experiment, the output current of the $\text{Al}_{0.25}\text{Ga}_{0.75}\text{N}/\text{GaN}$ HEMT is inversely proportional to the W , a larger W/L , and larger sensitive area can increase the output current and sensitivity, but long-term exposure of the large sensitive area to the air will reduce the stability due to increased interference from environmental uncertainties and power consumption. Therefore, only the testing results of the device at $W = 3 \mu\text{m}$ are demonstrated here as those results are representative. Figure 7a shows the current as a function of bias voltage from HEMTs with Ga_2O_3 in the gate region exposed to a series of solutions whose pH varied from 2 to 10 when the temperature was $20 \pm 2^\circ\text{C}$ and humidity $<85\%$.

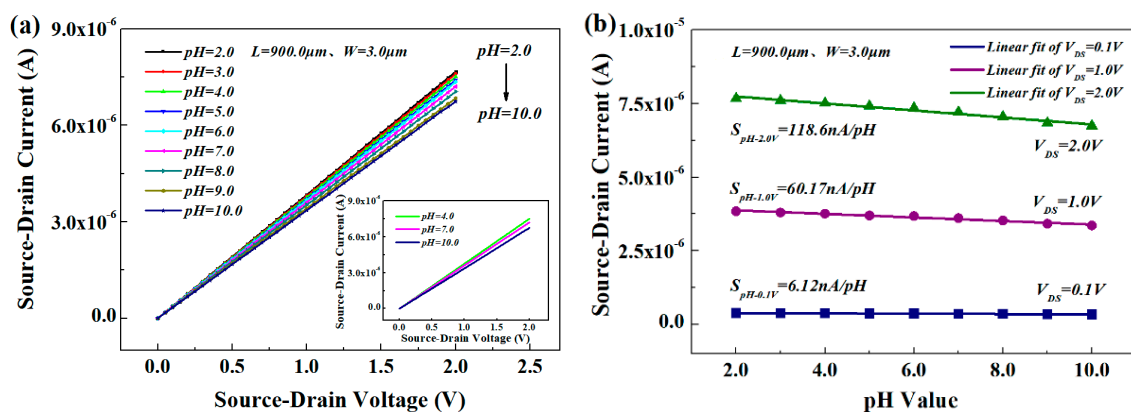


Figure 7. The sensitive characteristics of open-gated $\text{Al}_{0.25}\text{Ga}_{0.75}\text{N}/\text{GaN}$ HEMT-based sensor ($W = 3 \mu\text{m}$) in different pH solutions: (a) I_{DS} - V_{DS} with different pH values; (b) I_{DS} -pH with different V_{DS} values.

The adsorption of polar molecules on the surface of the HEMT affected the surface potential and device characteristics, and the current was significantly increased upon exposure to these polar liquids as pH decreased. The I_{DS} in each case can be extracted and plotted as a function of pH value (Figure 7b), and the sensitivity was $0.06 \mu\text{A/V}\cdot\text{pH}$ and the maximum accuracy was 0.1 pH. Figure 7 shows that the HEMT-based pH sensor with the Ga_2O_3 gate dielectric is sensitive to the concentration of the polar liquid and therefore could be used to differentiate between liquids into which a small amount of leakage of another substance has occurred.

Figure 8 is the static characteristics of the open-gated $\text{Al}_{0.25}\text{Ga}_{0.75}\text{N}/\text{GaN}$ HEMT-based pH sensor under different V_{DS} and different pH, which are the linearity, hysteresis, and repeatability characteristics of the sensor for three cycles of forward (input-increased) and backward (input-decreased) calculated using MATLAB. The experimental results showed that under a constant pH = 7, V_{DS} changed from 0 V to 2.0 V and 2.0 V to 0 V, the sensor had excellent nonlinearity, repeatability, and hysteresis characteristics, which were 0.06%F.S., 0.14%F.S., and 0.56%F.S., respectively (Figure 8a). This indicates that the sensor could work under different bias voltages and had excellent stability. Furthermore, when the pH values changed from 2 to 10 and 10 to 2, the nonlinearity, hysteresis, and repeatability were 15.33%F.S., 4.28%F.S., and 8.92%F.S. at $V_{DS} = 1.0$ V (Figure 8b), respectively. The result was not as perfect as the result in Figure 8a, which may be affected by the defects and surface states of the natural metal oxide Ga_2O_3 material on the sensitive surface of the sensor [43,44], but this does not affect the sensor's suitability for repeated measurements with different pH values and satisfying different changes in acid and alkaline solutions.

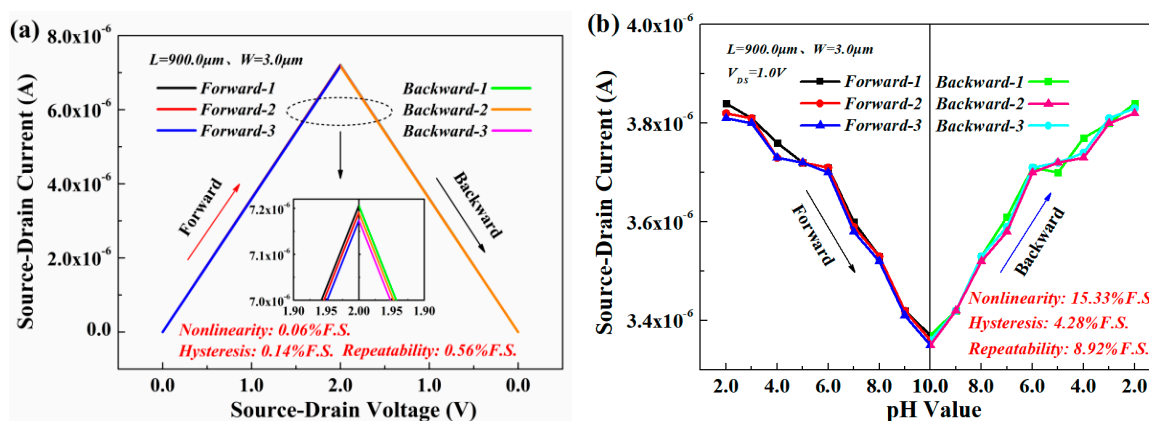


Figure 8. The analysis of the static characteristics of the open-gated $\text{Al}_{0.25}\text{Ga}_{0.75}\text{N}/\text{GaN}$ HEMT-based pH sensor: (a) I_{DS} - V_{DS} at pH = 7.0; (b) I_{DS} -pH at $V_{DS} = 1.0$ V.

The real-time I_{DS} measurements were also performed with the changing pH solutions, as shown in Figure 9. The I_{DS} of the sensor in acid solution (pH = 4), neutral solution (pH = 7), and alkaline solution (pH = 10) was measured at $V_{DS} = 1.0$ V, respectively. Each pH value is measured every 5 s for a total of 50 measurements. From the figure, the sensor shows excellent sensitivity and stability characteristics, which is attributed to the narrow channel of the $\text{Al}_{0.25}\text{Ga}_{0.75}\text{N}/\text{GaN}$ HEMT sensor and the integrated packaging microchannel to avoid the larger sensitive area from being disturbed by environmental interference and to ensure the quality of the oxide in the sensitive area and larger H^+ and HO^- concentration. Furthermore, according to the test statistics, after more than 200 measurements, the characteristics of the pH sensor could be restored to 99.36% of the initial current after being cleaned with DI water and placed at room temperature for 1 h.

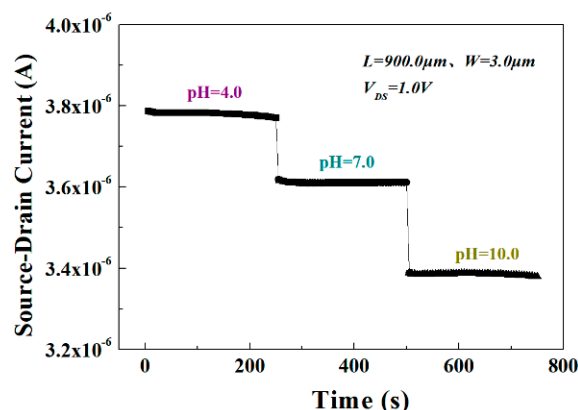


Figure 9. I_{DS} response of the open-gated $\text{Al}_{0.25}\text{Ga}_{0.75}\text{N}/\text{GaN}$ HEMT-based pH sensor during real-time measurement of the pH value from 4 to 10 at $V_{DS} = 1.0$ V with the time interval of 5 s.

In order to further promote the development of monolithic integrated multi-function sensors and integrated circuits (IC), the development of a low power consumption sensor device is highly important in the future. Therefore, the research into low-power sensors becomes more and more important with the development of IC manufacturing technology. Reducing the output current is a means to achieve low power consumption, so the sensor in this article used a smaller sensitive area width to length ratio. At the same time, a GaN cap layer was added to the basic structure of the sensor, which could increase the mobility of 2DEG at the expense of a slight decrease in carrier concentration under the polarization effect.

On the other hand, the GaN cap layer could increase the Schottky barrier on the AlGaIn/GaN heterojunction structure, thereby significantly reducing gate leakage [45]. Of course, the sensor designed in this article was an open-gated structure, so there was no gate leakage and gate power consumption. Figure 10 shows the power consumption of the $\text{Al}_{0.25}\text{Ga}_{0.75}\text{N}/\text{GaN}$ HEMT-based pH sensor under different V_{DS} in the range of pH = 2 to 10. When $V_{DS} = 0.1$ V, 1.0 V, and 2.0 V, the average value of P was 0.18 μW , 3.62 μW , and 14.5 μW , respectively. The small size and low power consumption of this sensor enabled the small-sized substrate to easily accommodate multiple sensors to monitor the pH, temperature, humidity, and air quality of the environment.

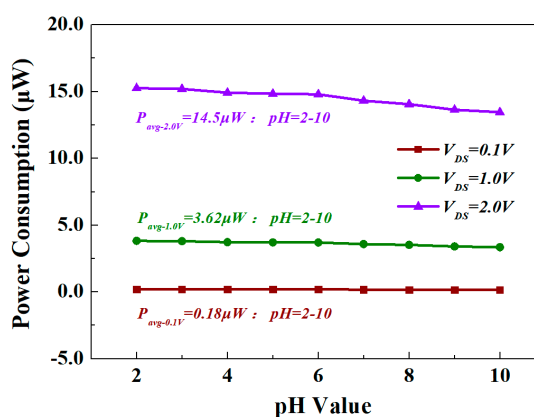


Figure 10. The power consumption of the $\text{Al}_{0.25}\text{Ga}_{0.75}\text{N}/\text{GaN}$ HEMT-based pH sensor under different V_{DS} in the range of pH = 2 to 10.

Table 1 gives the main characteristic parameters of the $\text{Al}_{0.25}\text{Ga}_{0.75}\text{N}/\text{GaN}$ HEMT-based pH sensor and mainly includes the key geometric structure parameters (W , integration) and performance parameters (Sensitivity- S_{pH} , Nonlinearity- N_L , Hysteresis- H , Repeatability- R , Power consumption- P , Detection range- D_r , Resolution- r , and lifetime- L_t).

Table 1. The main characteristic parameters of the Al_{0.25}Ga_{0.75}N/GaN HEMT-based pH sensor.

Main Characteristics	Parameter ($V_{DS} = 1.0$ V)	Values	Units
Channel width	W	3	μm
Integration		30	
Sensitivity	S_{pH}	0.06	$\mu\text{A/V}\cdot\text{pH}$
Nonlinearity	N_L	15.33	%F.S.
Hysteresis	H	4.28	%F.S.
Repeatability	R	8.92	%F.S.
Power consumption	P	<5.0	μW
Detection range	D_r	2.0–10.0	pH
Resolution	r	0.1	pH
Lifetime	L_t	>200	times

5. Conclusions

Al_{0.25}Ga_{0.75}N/GaN HEMT-based pH sensors with open gate and narrow channel width were fabricated and characterized. The open-gated HEMT could improve the control ability of the heterojunction channel 2DEG by the change in charge and potential in the sensitive area. Additionally, the narrow channel sensor has a relatively small output current, which can reduce its power consumption. The pH sensitivity of the sensor could reach 0.06 $\mu\text{A/V}\cdot\text{pH}$ in the range of pH = 2 to 10, resolution was 0.1 pH, and it had ultra-low power (<5.0 μW) and small hysteresis in multiple measurements at $V_{DS} = 1.0$ V. Moreover, the performance of the HEMT-based pH sensor system could be improved in a microchannel, which could be attributed to better surface Ga_xO_y in a microchannel with larger H⁺ and HO[−] concentration on the sensing surface. The sensitivity of sensors with the narrow channel was slightly inferior than that of the sensors with a wide channel. However, this kind of sensor with a narrow channel has the virtue of lower power consumption and excellent stability, which can be widely used in various unattended and harsh environments. Moreover, the features of integration and intelligence provide unlimited prospects for in-body online monitoring.

Author Contributions: All authors discussed and agreed upon the idea, and made scientific contributions: Writing—original draft preparation, X.Y., J.A., and X.L.; Experiment designing, X.L., W.L., C.H., and S.M.; Experiment performing, X.Y. and S.W.; Data analysis, X.Y. and J.A.; Writing—review and editing, X.Y., X.L., and L.H. All authors have read and agreed to the published version of the manuscript.

Funding: This work was supported in part by the National Natural Science Foundation of China under Grant 51625504, Grant 51707062 and Grant 61671368, and in part by Science and Technology Planning Project of Zhejiang Province, China under Grant 2017C31087.

Acknowledgments: Some SEM and Raman work were done at the International Center for Dielectric Research (ICDR) and Instrumental Analysis Center, Xi'an Jiaotong University, Xi'an, China. The authors would also like to Dai and Yang for their help in using the SEM.

Conflicts of Interest: The authors declare no conflict of interest.

References

- Huber, A.; Demartis, S.; Neri, D. The use of biosensor technology for the engineering of antibodies and enzymes. *J. Mol. Recognit.* **1999**, *12*, 198–216. [[CrossRef](#)]
- Toldrà, A.; Alcaraz, C.; Diogène, J.; O'Sullivan, C.K.; Campàs, M. Detection of *Ostreopsis cf. ovata* in environmental samples using an electrochemical DNA-based biosensor. *Sci. Total. Environ.* **2019**, *689*, 655–661. [[CrossRef](#)] [[PubMed](#)]
- Atci, E.; Babauta, J.T.; Sultana, S.T.; Beyenal, H. Microbiosensor for the detection of acetate in electrode-respiring biofilms. *Biosens. Bioelectron.* **2016**, *81*, 517–523. [[CrossRef](#)] [[PubMed](#)]
- Maduraiveeran, G.; Sasidharan, M.; Ganesan, V. Electrochemical sensor and biosensor platforms based on advanced nanomaterials for biological and biomedical applications. *Biosens. Bioelectron.* **2018**, *103*, 113–129. [[CrossRef](#)] [[PubMed](#)]

5. Vigneshvar, S.; Sudhakumari, C.C.; Senthilkumaran, B.; Prakash, H. Recent Advances in Biosensor Technology for Potential Applications An Overview. *Front. Bioeng. Biotechnol.* **2016**, *4*, 11. [\[CrossRef\]](#)
6. Alonso-Lomillo, M.A.; Domínguez-Renedo, O. Screen-Printed Biosensors in Drug Analysis. *Curr. Pharm. Anal.* **2017**, *13*, 169–174. [\[CrossRef\]](#)
7. Marrakchi, M.; Dzyadevych, S.V.; Namour, P.; Martelet, C.; Jaffrezic-Renault, N. A novel proteinase K biosensor based on interdigitated conductometric electrodes for proteins determination in rivers and sewers water. *Sensors Actuators B: Chem.* **2005**, *111*, 390–395. [\[CrossRef\]](#)
8. Adaszewska, A.; Kalińska-Bienias, A.; Jagielski, P.; Woźniak, K.; Kowalewski, C. The use of BIOCHIP mosaics in diagnostics of bullous pemphigoid: Evaluation and comparison to conventional multistep procedures. *J. Cutan. Pathol.* **2019**, *47*, 121–127. [\[CrossRef\]](#)
9. Pearton, S.; Ren, F.; Wang, Y.-L.; Chu, B.; Chen, K.; Chang, C.; Lim, W.; Lin, J.; Norton, D. Recent advances in wide bandgap semiconductor biological and gas sensors. *Prog. Mater. Sci.* **2010**, *55*, 1–59. [\[CrossRef\]](#)
10. Ren, F.; Pearton, S.J. Sensors using AlGaIn/GaN based high electron mobility transistor for environmental and bio-applications. *Phys. Status Solidi* **2012**, *9*, 393–398. [\[CrossRef\]](#)
11. Cimalla, V. *Label-Free Biosensors Based on III-Nitride Semiconductors*; Springer Series on Chemical Sensors and Biosensors; Springer: New York, NY, USA, 2017; pp. 59–102.
12. Khanna, K.V. Robust HEMT microsensors as prospective successors of MOSFET/ISFET detectors in harsh environments-HEMT microsensors. *Front. Sens.* **2013**, *1*, 38–48.
13. Chaniotakis, N.; Sofikiti, N. Novel semiconductor materials for the development of chemical sensors and biosensors: A review. *Anal. Chim. Acta* **2008**, *615*, 1–9. [\[CrossRef\]](#) [\[PubMed\]](#)
14. Strite, T.; Morkoc, H. GaN, AlN, and InN: A review. *J. Vac. Science Technol. B Microelectron. Nanometer Struct.* **1998**, *10*, 1237–1266. [\[CrossRef\]](#)
15. Ould-Abbas, A.; Zeggai, O.; Bouchaour, M.; Trari, D.; Madani, M.; Sahouane, N.; Nisa, E.S.; Oussama, Z. Study on functionalizing the surface of AlGaIn/GaN high electron mobility transistor based sensors. *J. Optoelectron. Adv. Mater.* **2013**, *15*, 1323–1327.
16. Rais-Zadeh, M.; Gokhale, V.J.; Ansari, A.; Faucher, M.; Theron, D.; Cordier, Y.; Buchaillet, L. Gallium Nitride as an Electromechanical Material. *J. Microelectromechanical Syst.* **2014**, *23*, 1252–1271. [\[CrossRef\]](#)
17. Xue, D.; Zhang, H.; Ahmad, A.U.; Liang, H.; Liu, J.; Xia, X.; Guo, W.; Huang, H.; Xu, N. Enhancing the sensitivity of the reference electrode free AlGaIn/GaN HEMT based pH sensors by controlling the threshold voltage. *Sensors Actuators B Chem.* **2020**, *306*, 127609. [\[CrossRef\]](#)
18. Nigam, A.; Bhat, T.N.; Bhati, V.S.; Bin Dolmanan, S.; Tripathy, S.; Kumar, M. MPA-GSH Functionalized AlGaIn/GaN High-Electron Mobility Transistor-Based Sensor for Cadmium Ion Detection. *IEEE Sens. J.* **2019**, *19*, 2863–2870. [\[CrossRef\]](#)
19. Alifragis, Y.; Volosirakis, A.; Chaniotakis, N.A.; Konstantinidis, G.; Iliopoulos, E.; Georgakilas, A. AlGaIn/GaN high electron mobility transistor sensor sensitive to ammonium ions. *Phys. Status Solidi (a)* **2007**, *204*, 2059–2063. [\[CrossRef\]](#)
20. Liu, X.; Zhao, L.; Miao, B.; Gu, Z.; Wang, J.; Peng, H.; Li, J.; Sun, W.; Li, J. Wearable Multiparameter Platform Based on AlGaIn/GaN High-electron-mobility Transistors for Real-time Monitoring of pH and Potassium Ions in Sweat. *Electroanalysis* **2020**, *32*, 422–428. [\[CrossRef\]](#)
21. Espinosa, N.; Schwarz, S.U.; Cimalla, V.; Ambacher, O. Detection of different target-DNA concentrations with highly sensitive AlGaIn/GaN high electron mobility transistors. *Sens. Actuators B Chem.* **2015**, *210*, 633–639. [\[CrossRef\]](#)
22. Schwarz, S.U.; Linkohr, S.; Lorenz, P.; Krischok, S.; Nakamura, T.; Cimalla, V.; Nebel, C.E.; Ambacher, O. DNA-sensor based on AlGaIn/GaN high electron mobility transistor. *Phys. Status solidi* **2011**, *208*, 1626–1629. [\[CrossRef\]](#)
23. Espinosa, N.; Schwarz, S.; Cimalla, V.; Podolska, A.; Ambacher, O. Dynamic Detection of Target-DNA with AlGaIn/GaN High Electron Mobility Transistors. *Procedia Eng.* **2015**, *120*, 908–911. [\[CrossRef\]](#)
24. Sarangadharan, I.; Regmi, A.; Chen, Y.-W.; Hsu, C.-P.; Chen, P.-C.; Chang, W.-H.; Lee, G.-Y.; Chyi, J.-I.; Shiesh, S.-C.; Lee, G.-B.; et al. High sensitivity cardiac troponin I detection in physiological environment using AlGaIn/GaN High Electron Mobility Transistor (HEMT) Biosensors. *Biosens. Bioelectron.* **2018**, *100*, 282–289. [\[CrossRef\]](#) [\[PubMed\]](#)

25. Wen, X.; Gupta, S.; Wang, Y.; Nicholson, T.R.; Lee, S.C.; Lu, W. High sensitivity AlGaIn/GaN field effect transistor protein sensors operated in the subthreshold regime by a control gate electrode. *Appl. Phys. Lett.* **2011**, *99*, 43701. [\[CrossRef\]](#)
26. Kang, B.S.; Ren, F.; Wang, L.; Lofton, C.M.; Tan, W.; Pearton, S.J.; Dabiran, A.M.; Osinsky, A.; Chow, P.P. Electrical detection of immobilized proteins with ungated AlGaIn/GaN high-electron-mobility Transistors. *Appl. Phys. Lett.* **2005**, *87*, 023508. [\[CrossRef\]](#)
27. Lee, C.-T.; Chiu, Y.-S. Photoelectrochemical passivated ZnO-based nanorod structured glucose biosensors using gate-recessed AlGaIn/GaN ion-sensitive field-effect-transistors. *Sens. Actuators B Chem.* **2015**, *210*, 756–761. [\[CrossRef\]](#)
28. Chu, B.H.; Byong, K.S.; Hung, S.C.; Sheng, C.H.; Ke, H.C.; Fan, R.; Andrew, S.; Brent, P.; Gila, S.; Pearton, S.J. Aluminum gallium nitride (AlGaIn)/GaN high electron mobility transistor-based sensors for glucose detection in exhaled breath condensate. *J. Diabetes Sci. Technol.* **2010**, *4*, 171–179. [\[CrossRef\]](#)
29. Li, J.-D.; Cheng, J.-J.; Miao, B.; Wei, X.-W.; Xie, J.; Zhang, J.-C.; Zhang, Z.-Q.; Li, H.-W.; Wu, D.-M. Label free electrical detection of prostate specific antigen with millimeter grade biomolecule-gated AlGaIn/GaN high electron mobility transistors. *Microsyst. Technol.* **2014**, *21*, 1489–1494. [\[CrossRef\]](#)
30. Li, J.-D.; Cheng, J.-J.; Miao, B.; Wei, X.-W.; Xie, J.; Zhang, J.-C.; Zhang, Z.-Q.; Wu, D.-M. Detection of prostate-specific antigen with biomolecule-gated AlGaIn/GaN high electron mobility transistors. *J. Micromech. Microeng.* **2014**, *24*, 75023. [\[CrossRef\]](#)
31. Kang, B.S.; Wang, H.T.; Lele, T.P.; Tseng, Y.; Ren, F.; Pearton, S.J.; Johnson, J.W.; Rajagopal, P.; Roberts, J.C.; Piner, E.L.; et al. Prostate specific antigen detection using AlGaIn/GaN high electron mobility transistors. *Appl. Phys. Lett.* **2007**, *91*, 112106. [\[CrossRef\]](#)
32. Pulikkathodi, A.K.; Sarangadharan, I.; Hsu, C.-P.; Chen, Y.-H.; Hung, L.-Y.; Lee, G.-Y.; Chyi, J.-I.; Lee, G.-B.; Wang, Y.-L. Enumeration of circulating tumor cells and investigation of cellular responses using aptamer-immobilized AlGaIn/GaN high electron mobility transistor sensor array. *Sens. Actuators B Chem.* **2018**, *257*, 96–104. [\[CrossRef\]](#)
33. Steinhoff, G.; Hermann, M.; Schaff, W.J.; Eastman, L.F.; Stutzmann, M.; Eickhoff, M. pH response of GaN surfaces and its application for pH-sensitive field-effect transistors. *Appl. Phys. Lett.* **2003**, *83*, 177–179. [\[CrossRef\]](#)
34. Kang, B.S.; Wang, H.T.; Ren, F.; Gila, B.P.; Abernathy, C.R.; Pearton, S.J.; Johnson, J.W.; Rajagopal, P.; Roberts, J.C.; Piner, E.L.; et al. pH sensor using AlGaIn/GaN high electron mobility transistors with Sc₂O₃ in the gate region. *Appl. Phys. Lett.* **2007**, *91*, 012110. [\[CrossRef\]](#)
35. Chen, C.-C.; Chen, H.-I.; Liu, H.-Y.; Chou, P.-C.; Liou, J.-K.; Liu, W.-C. On a GaN-based ion sensitive field-effect transistor (ISFET) with a hydrogen peroxide surface treatment. *Sens. Actuators B Chem.* **2015**, *209*, 658–663. [\[CrossRef\]](#)
36. Dong, Y.; Son, D.-H.; Dai, Q.; Lee, J.-H.; Won, C.-H.; Kim, J.-G.; Kang, S.-H.; Lee, J.-H.; Dunjun, C.; Lu, H.; et al. AlGaIn/GaN heterostructure pH sensor with multi-sensing segments. *Sens. Actuators B Chem.* **2018**, *260*, 134–139. [\[CrossRef\]](#)
37. Liuan, L.; Xiaobo, L.; Taofei, P.; Liu, Y.; Ao, J.-P. Normally off AlGaIn/GaN ion-sensitive field effect transistors realized by photoelectron chemical method for pH sensor application. *Superlattices Microstruct.* **2019**, *128*, 99–104.
38. Anvari, R.; Myers, M.; Umana-Membreno, G.A.; Baker, M.V.; Spagnoli, D.; Parish, G.; Nener, B.D. Charging mechanism of AlGaIn/GaN open-gate pH sensor and electrolyte interface. In Proceedings of the Conference on Optoelectronic and Microelectronic Materials and Devices, Perth, Australia, 14–17 December 2014; pp. 156–159. [\[CrossRef\]](#)
39. Yates, D.E.; Levine, S.; Healy, T.W. Site-binding model of the electrical double layer at the oxide/water interface. *J. Chem. Soc. Faraday Trans. 1 Phys. Chem. Condens. Phases* **1974**, *70*, 1807–1818. [\[CrossRef\]](#)
40. Colin, W.D.J. *Polarization Effects in Semiconductors: From Ab Initio Theory to Device Applications*; Wood, C., Jena, D., Eds.; Springer: New York, NY, USA, 2007.
41. Ma, S.; Lee, Y.-K.; Zhang, A.; Li, X. Label-free detection of Cordyceps sinensis using dual-gate nanoribbon-based ion-sensitive field-effect transistor biosensor. *Sens. Actuators B Chem.* **2018**, *264*, 344–352. [\[CrossRef\]](#)

42. Ma, S.; Li, X.; Lee, Y.-K.; Zhang, A. Direct label-free protein detection in high ionic strength solution and human plasma using dual-gate nanoribbon-based ion-sensitive field-effect transistor biosensor. *Biosens. Bioelectron.* **2018**, *117*, 276–282. [[CrossRef](#)]
43. Bousse, L.J.; Vlekkert, H.V.D.; De Rooij, N. Hysteresis in Al_2O_3 -gate ISFETs. *Sensors Actuators B Chem.* **1990**, *2*, 103–110. [[CrossRef](#)]
44. Liu, H.-Y.; Hsu, W.-C.; Chen, W.-F.; Lin, C.-W.; Li, Y.-Y.; Lee, C.-S.; Sun, W.-C.; Wei, S.-Y.; Yu, S.-M. Investigation of AlGaIn/GaN Ion-Sensitive Heterostructure Field-Effect Transistors-Based pH Sensors with Al_2O_3 Surface Passivation and Sensing Membrane. *IEEE Sens. J.* **2016**, *16*, 3514–3522. [[CrossRef](#)]
45. Yu, E.T.; Dang, X.Z.; Yu, L.S.; Qiao, D.; Asbeck, P.M.; Lau, S.S.; Sullivan, G.J.; Boutros, K.S.; Redwing, J.M. Schottky barrier engineering in III–V nitrides via the piezoelectric effect. *Appl. Phys. Lett.* **1998**, *73*, 1880–1882. [[CrossRef](#)]

Publisher's Note: MDPI stays neutral with regard to jurisdictional claims in published maps and institutional affiliations.



© 2020 by the authors. Licensee MDPI, Basel, Switzerland. This article is an open access article distributed under the terms and conditions of the Creative Commons Attribution (CC BY) license (<http://creativecommons.org/licenses/by/4.0/>).